nature astronomy

Article

https://doi.org/10.1038/s41550-022-01882-x

Orbit-to-ground framework to decode and predict biosignature patterns in terrestrial analogues

In the format provided by the authors and unedited

Supplementary Information

Microbial Ecology Methods Supplementary Data

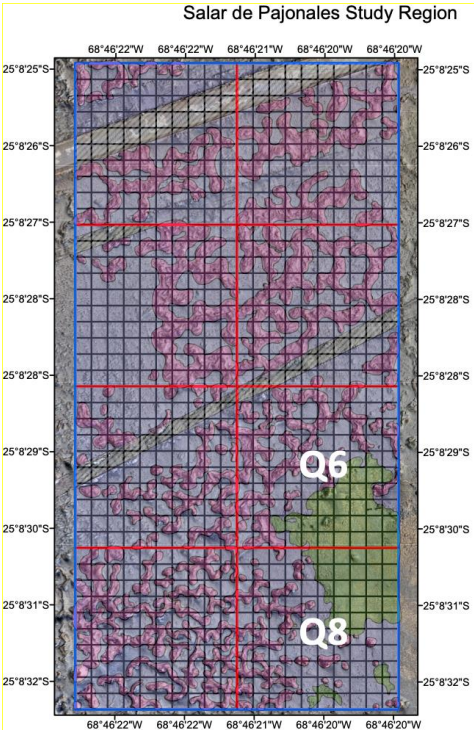

Supplementary Fig. 1. UAV image of the Dome Field. To investigate the effect of spatial scale on the probability for photosynthetic microbial community biosignatures (as % col) the study location was subdivided into nested hierarchical scales of study, including quadrants (red grid, 50m x 50 m), areas (black grid, 5 m x 5 m), and micro-sites (see Methods). UAV imagery was initially classified as raised areas (ridges and domes) or 'flat' areas [aeolian cover (grey) and patterned ground (green). Initial study hypotheses (H_0) were that i) biosignatures (%Col) varied significantly by spatial scale and ii) that 'raised' geomorphic features (perhaps linked to preferential water availability or more suitable rock architecture for colonization)[8,92,93,94] were more habitable for photosynthetic microbial communities than flat features, i.e., that geomorphic unit/ecological habitat type controlled biosignature probabilities at multiple scales. These habitat classifications were refined as an understanding of the features and associated microbial communities evolved. Furthermore, the 'abiotic' patterned ground observed in 2016 by aerial imagery (green unit) was in 2018 ground surveys ascertained to be micro-structures with living photosynthetic biological soil crust communities (BSC). To accommodate these new findings, we created micro-structure and bare salar surface micro-habitat and BSC biological morphotype categories and separated these data from the endolithic colonization mode analyses.

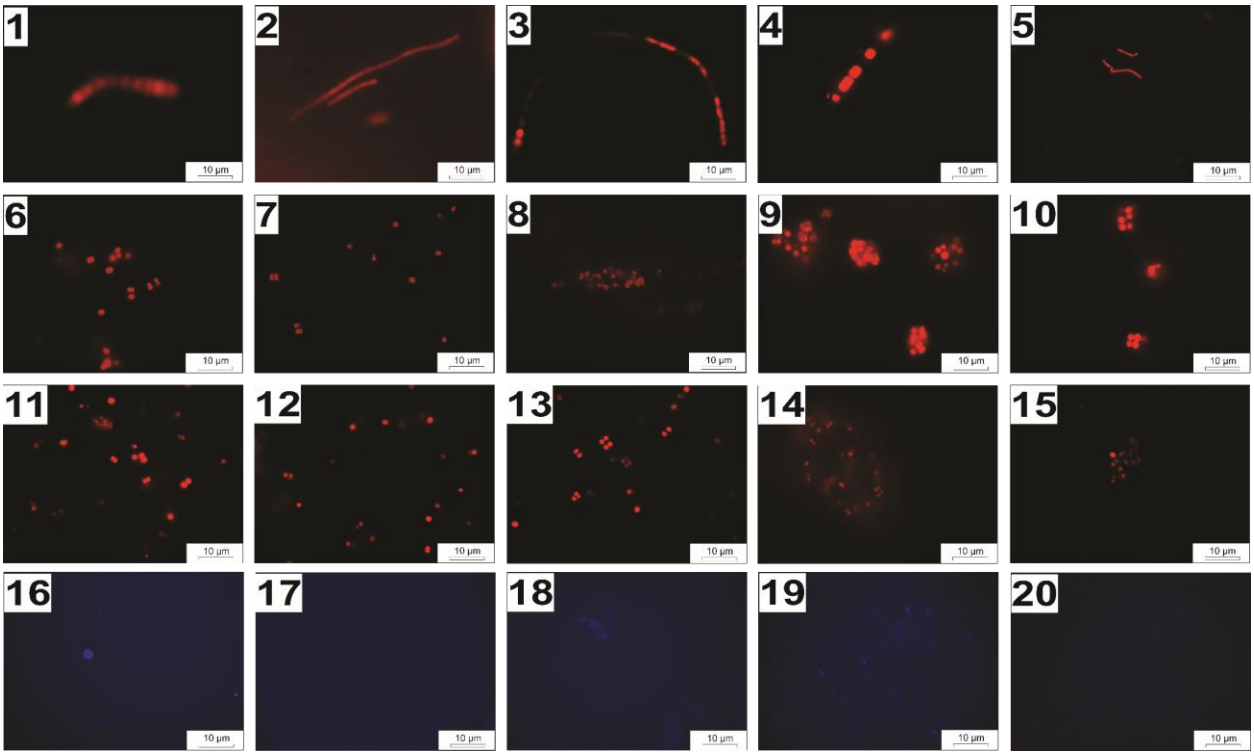

Supplementary Fig. 2. Confocal Laser Scanning Microscopy autofluorescence cell counts in green and orange pigmented biosignature layers (1-15) versus white (16-20) layers confirmed 4.49 $x10^5$ ± 2.83 $x10^5$ cells per mL and zero cells per mL, respectively.

Microbial Ecology Statistical Results Supplementary Data

Spatial Randomness/Aggregation Analyses (Ripley's K, Global Moran's I)

Ripley's K and Global Moran's I revealed non-random/aggregated/clustered (i.e., hotspots, islands, refugia)[27,115,116,117] spatial distributions for endolithic and BSC communities at all scales assessed.

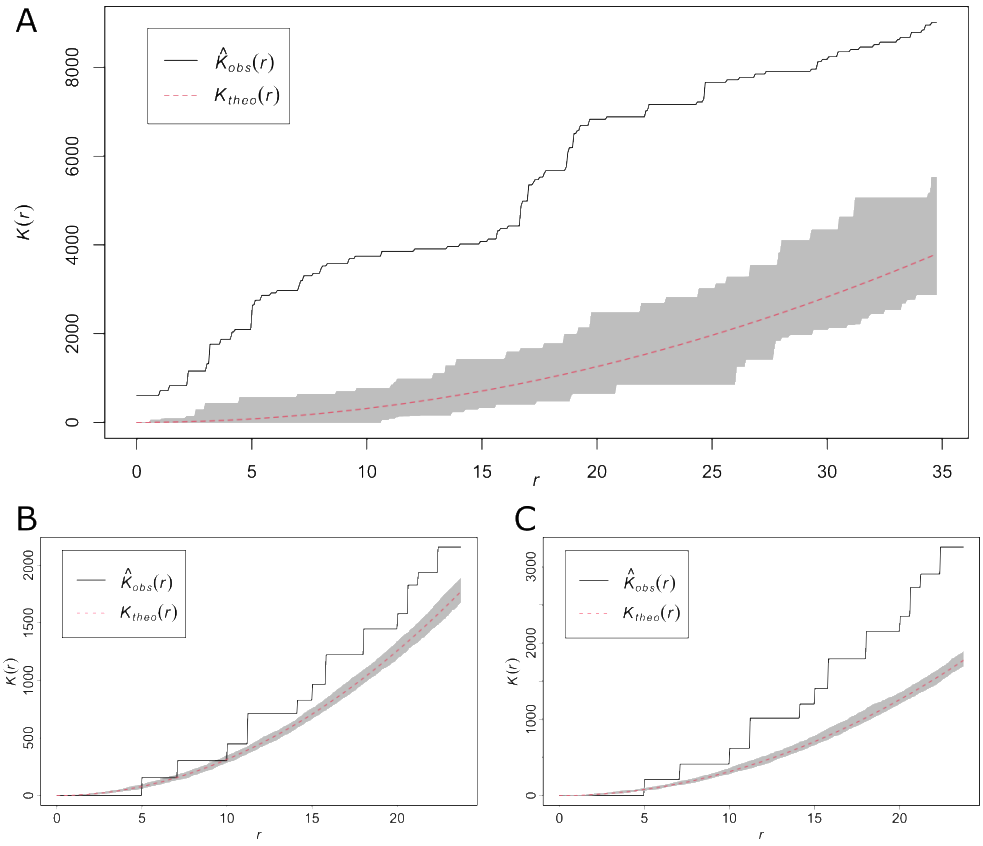

Supplementary Fig. 3. Spatial statistical analyses reveal clustering at multiple scales. **a,** The clustering pattern of endolithic microbial community biosignatures at larger scales examined (ES-1, distances (r) ≤35 m) is indicated by the observed K(r) values (solid line) above the theoretical envelope, as indicated by the red dotted line and the grey band showing the maximum and minimum values from 99 simulations. The envelope represents the variability of the complete spatial randomness (CSR) process, as the null hypothesis. In other words, our analysis showed more clustering than a homogenous Poisson process (CSR) would predict at this scale. **b, c,** Spatial pattern at fine-scales (≤20 cm) for endolithic biosignatures (**b**, ES-3 dome) and endoliths + BSC biosignatures (**c**, ES-3 aeolian cover) are also more clustered than CSR. These observations are also supported by Global Moran's I, which showed significant spatial autocorrelation (Monte-Carlo simulation of Moran's I, 1000 permutations, I = 0.03924 (ES1-2); 0.12947 (ES-3 dome); 0.26812 (ES-3 aeolian cover), p-value = 0.001 for all).

Pivot Table Statistics and Decision-Trees

Pivot-tables count the number of events, where in this case for Pajonales each event is some combination of microhabitat (e.g., alabaster, sand) and biosignature (endolith, BSC). A decision-tree is derived from the pivot-table, such that a sequence of yes/no decisions per microhabitat optimize the likelihood of detecting life/biosignatures in the fewest decisions possible. For example, based on the decision tree shown in Extended Data Fig. 3, alabaster microhabitats (in a dome macrohabitat) maximize the likelihood of observing endolithic biosignatures. Therefore, given this knowledge, at Pajonales, a rover programmed with a CNN algorithm might scan the environment with spectrometers for alabaster microhabitats, which have the highest probability for containing endolithic (or BSC) biosignatures.

Supplementary Table 1. Pivot table results for the probability of endolithic biosignatures (%Col) in the dome macrohabitat.

				Endolith Present (1), Absent (0)					
Geologic material/microhabitat				*0*		*1*		*Total*	
Alabaster	T2 crystal	T1 crystal	Sand	%	Count	%	Count	%	count
0	0	0	0	100	33			100	13
			1	100	8			100	8
		0 total		**100**	**41**			**100**	**41**
		1	0	69.54	137	30.46	60	100	197
		1 total		**69.54**	**137**	**30.46**	**60**	**100**	**197**
	0 total			**74.79**	**178**	**25.21**	**60**	**100**	**238**
	1	0	0	17.78	24	82.22	111	100	135
		0 total		**17.78**	**24**	**82.22**	**111**	**100**	**135**
	1 total			**17.78**	**24**	**82.22**	**111**	**100**	**135**
0 total				**54.16**	**202**	**45.84**	**171**	**100**	**373**
1	0	0	0			100	27	100	27
		0 total				**100**	**27**	**100**	**27**
	0 total					**100**	**27**	**100**	**27**
1 total						**100**	**27**	**100**	**27**
Total				**50.50**	**202**	**49.50**	**198**	**100**	**400**

In above table, data from the ecological survey (ES-3 above) are shown as follows: the absence of colonization, i.e., biosignatures, is registered as a "0" and the presence of endolithic community biosignatures as a "1" for each microhabitat (alabaster, Type II (T2) crystal, Type I (T1) crystal and sand) in the dome macrohabitat. As an example, of the n=400 total samples, n=8 samples were sand microhabitat, of which 100% were uncolonized, i.e., no biosignature present (n=8 with a count of "0" endolith biosignature).

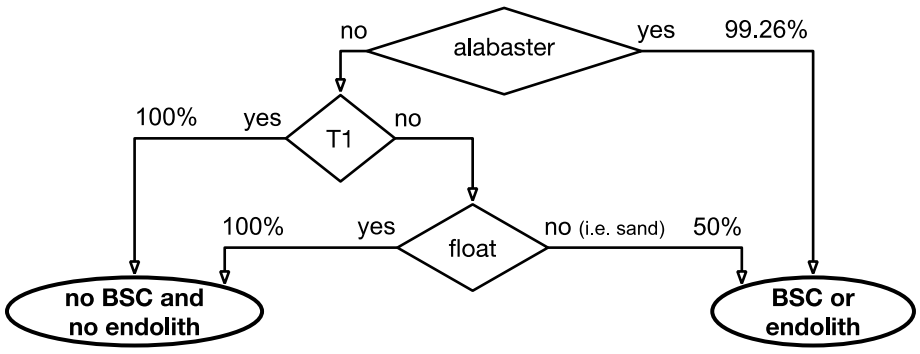

Supplementary Fig. 4. Rules for the probability a sample contains endolithic or BSC biosignatures in microhabitats of aeolian cover macrohabitat. The above is a visual representation of the main results of Supplementary Data Table 2. For instance, in the first decision in the figure, if the microhabitat is alabaster, then the probability of endolithic and/or BSC biosignatures present in a sample is 99.26% (%Col is: 135 colonized samples/136 total alabaster samples x100). If the microhabitat is not alabaster, this leads to the next decision choice of whether the microhabitat is a Type I (T1) crystal or not, and so forth.

Supplementary Table 2. Pivot table results for the probabilities of endolithic and/or BSC biosignatures (%Col) in microhabitats of the aeolian cover macrohabitat.

				BSC or Endolith Present (1), Absent (0)					
Geologic material/microhabitat				*0*		*1*		*Total*	
Alabaster	T1 crystal	Float	Sand	%	Count	%	Count	%	count
0	0	0	1	50	113	50	113	100	226
		0 total		**50**	**113**	**50**	**113**	**100**	**226**
		1	0	100	86			100	86
		1 total		**100**	**86**			**100**	**86**
	0 total			**63.78**	**199**	**36.22**	**113**	**100**	**312**
	1	0	0	100	3			100	3
		0 total		**100**	**3**			**100**	**3**
		1	0	100	25			100	25
		1 total		**100**	**25**			**100**	**25**
	1 total			**100**	**28**			**100**	**28**
0 total				**66.76**	**227**	**33.24**	**113**	**100**	**340**
1	0	0	0	0.74	1	99.26	135	100	136
		0 total		**0.74**	**1**	**99.26**	**135**	**100**	**136**
	0 total			**0.74**	**1**	**99.26**	**135**	**100**	**136**
1 total				**0.74**	**1**	**99.26**	**135**	**100**	**136**
Total				**47.90**	**228**	**51.10**	**248**	**100**	**476**

In the above table, data from the ecological survey (ES-3 above) are shown: counts for endolithic or BSC biosignatures (presence = "1", absence = "0") and counts (presence = "1", absence = "0") for each of the microhabitats (alabaster, T1 crystal, float and sand) in the aeolian cover macrohabitat.

GAM Models and Supplementary Data

Predictive model results for endolithic biosignatures in dome macro-habitat

Supplementary Table 3. Parameter estimates for the spatial logistic GAM. The response (dependent) variable is the absence/presence of endolithic colonization in 1 m x 1 m quadrat of dome face macro-habitat, with x,y spatial resolution at 5 cm x 5 cm. The predictor (independent) variables are the absence/presence of Type I (T1) crystal and Type II (T2) crystal micro-habitats, and the x-y coordinates of the 5 cm x 5 cm samples that form the 1 m x 1 m quadrat.

Coefficient	Estimate, β_j	Standard error	z-value	Odds ratio, $\exp(\beta_j)$	95% Confidence interval for odds ratio
Intercept	-3.4965	0.6606	-5.2931	0.030	(0.008; 0.110)
T1_1	3.5877	0.7517	4.7727	36.152	(8.284; 157.763)
T2_1	4.7733	0.7927	6.0217	118.315	(25.020; 559.484)

Interpretation of the model results: The model shows that the likelihood of endolithic biosignatures was 36 times greater in the T1 micro-habitats and 118 times greater in the T2 micro-habitat when compared to areas without T1 and T2 micro-habitats, respectively. In terms of probability, it is 97.3% more likely to observe endolithic biosignatures if T1 is present when compared to areas that do not have T1. Likewise, it is 99.16% more likely to observe endolithic biosignatures if T2 is present when compared to areas that do not have T2. If the odds ratio is greater than one, then the micro-habitat shows a greater association (or higher

likelihood of having endolithic biosignatures). If the odds ratio is less than one, the micro-habitat has a negative relationship with biosignatures (or a lower likelihood of having endolithic biosignatures present when compared to areas that do not have that micro-habitat).

Predictive models for endolithic and BSC biosignatures of aeolian cover

Endolithic Biosignatures in Aeolian Cover Macro-Habitat (Supplementary Table 4a): In the dome macro-habitat model above, sand micro-habitat was always negatively correlated with endolithic biosignatures (close to -1, i.e., sand was predominantly in areas where there was no endolithic biosignatures or the alabaster was bare) and was therefore not included in Methods eq. (1) above. However, in the aeolian cover macro-habitat, sand was observed in some areas where alabaster was also present and colonized by endoliths. This is illustrated in the probability contour map for endolithic biosignatures in the aeolian cover macro-habitat (Fig. 5d, right box).

BSC Biosignatures of Aeolian Cover Macro-Habitat (Supplementary Table 4b-d). In the aeolian cover macro-habitat, only alabaster or sand can be included in the model, not both. When both variables are included, the model will not converge because some combinations do not exist in the original dataset (see Supplementary Table 2). Indeed, as indicated below, the presence of sand was positively associated with, and increased the chances for, the presence of BSC biosignatures (Supplementary Table 4c). More specifically, in cases where both sand and alabaster are absent ("sand=0, alabaster=0"), there were no cases where BSC biosignatures was present. Conversely, BSC biosignatures will always be present if both sand and alabaster are present ("sand=1, alabaster=1"). Thus, both these conditions were removed from the models to ensure convergence. Below, we first examined sand and alabaster combinations in separate models (Supplementary Table 4b-c) and then created a model to consider situations with alabaster *only* and sand *only* (Supplementary Table 4d). The model (Supplementary Table 4d) that included alabaster *only* (without any sand) and sand *only* (without any alabaster) showed that the direction of the relationships to BSC biosignatures is consistent with those observed for Supplementary Table 4b-c. However, the magnitude of the association was much stronger when *both* micro-habitats were present in the same sample (Supplementary Table 4d).

Supplementary Table 4. GAM predictive models for endolithic (a) and BSC biosignatures in aeolian cover macro-habitat.

a). Estimated parameters for predicting likelihood of endolithic biosignatures in aeolian cover.					
Parametric Coefficients	Estimate, β_j	Standard error	z-value	Odds ratio, exp(β_j)	95% Confidence interval for odds ratio
Intercept	-92.7851	28.9458	-3.2055	5.06 e-41	(1.161 e-65; 2.204 e-16)
sand	-3.4207	1.0694	-3.1988	0.033	(0.004; 0.266)
Smooth term					
Term	edf	Ref,edf	χ^2-value	p-value	
f(x_coord,y_coord)	10.5	11.96	31.99	0.0014	
Model information					
Adjusted R^2 = 0.88	Deviance explained = 86.7%			n = 400	
b). Estimated parameters for predicting likelihood of BSC given presence of alabaster.					
A. Parametric Coefficients	Estimate, b_j	Standard error	z-value	Odds ratio, exp(b_j)	95% Confidence interval for odds ratio
Intercept	-11.8796	2.9134	-4.078	6.93 e-06	(2.295 e-08; 2.092 e-03)
Alabaster	-1.5913	0.6008	-2.649	0.2037	(0.063;0.661)
A. Smooth term					
Term	edf	Ref,edf	χ^2-value	p-value	

f(x_coord,y_coord)	12.69	14.58	46.6	< 0.0001	
B. Model information					
Adjusted R^2 = 0.56	Deviance explained = 56.5%			n = 400	

c). Estimated parameters for predicting likelihood of BSC given presence of sand.

Parametric Coefficients	Estimate, b_j	Standard error	z-value	Odds ratio, exp(b_j)	95% Confidence interval for odds ratio
Intercept	-39.4748	9.6868	-4.0751	7.183 e-18	(4.080 e-26; 1.265 e-09)
sand	9.3319	1.6123	5.7811	11292.567	(479.087; 266175.40)
Smooth term					
Term	edf	Ref,edf	χ^2-value	p-value	
f(x_coord,y_coord)	12.5	14.18	30.33	0.0087	
Model information					
Adjusted R^2 = 0.92	Deviance explained = 90.4%			n = 400	

d). Estimated parameters for predicting the likelihood of BSC for sand *only* and alabaster *only*.

Parametric Coefficients	Estimate, β_j	Standard error	z-value	Odds ratio, exp(β_j)	95% Confidence interval for odds ratio
Intercept	-21.4441	5.2621	-4.075	4.86 e-10	(1.614e-14; 1.466 e-05)
Alabaster only (no sand)	-5.0169	0.7144	-7.023	0.0066	(0.002; 0.027)
Sand only (no alabaster)	2.5901	1.0267	2.523	13.3305	(1.782; 99.727)
Smooth term					
Term	edf	Ref,edf	χ^2-value	p-value	
f(x_coord,y_coord)	11.45	13.12	43.43	< 0.0001	
Model information					
Adjusted R^2 = 0.83	Deviance explained = 80.5%			n = 400	

a, Results for GAM for endolithic biosignatures in aeolian cover macro-habitat. Estimated parameters for predicting the likelihood of endolithic biosignatures (absent, present) in the 1 m x 1 m quadrat of aeolian cover, with x,y spatial resolution at 5 cm x 5 cm. The predictors are the presence of sand (1=yes, 0=no) and the x-y coordinates of the 5 cm x 5 cm samples in the 1 m x 1 m quadrat. Interpretation of the model results: Supplementary Table 4a shows that sand is negatively associated with the presence of endolithic biosignatures. When sand was observed where alabaster was also present, there was a 30-fold ($1/OR_{sand}=1/0.033$) decrease in observing endolithic biosignatures. We hypothesize this finding is related to light effects, where a layer of alabaster that is covered by sand has significantly lower light penetration, making it a less suitable habitable micro-environment for endolithic colonization; **b, Estimated parameters for predicting the likelihood of BSC biosignatures given the presence of alabaster**. In this GAM model, alabaster is denoted as present if the 5 cm x 5 cm sample area contains *alabaster micro-habitat and alabaster/sand mix* (i.e., the latter is when *both* micro-habitats are present in a sample) in a 1 m x 1 m quadrat of aeolian cover, with x,y spatial resolution at 5 cm x 5 cm. In this model, alabaster micro-habitat present = yes, alabaster and sand micro-habitat both present = yes; all other conditions = no; **c, Estimated parameters for predicting the likelihood of BSC biosignatures given the presence of sand**. In this GAM model, sand micro-habitat is denoted as present if the 5 cm x 5 cm sample area contains *sand or sand/alabaster mix* (i.e., the latter is when *both* micro-habitats are present in the sample) in a 1 m x 1 m quadrat of aeolian cover, with x,y spatial resolution at 5 cm x 5 cm. In this model, sand micro-habitat only = yes; sand and alabaster micro-habitats both present = yes; all other conditions = no; **d) Estimated parameters for predicting the likelihood of BSC biosignatures**. This GAM model considers the presence of *sand only* (sand only = yes; all other conditions = no) and *alabaster only* (alabaster only = yes; all other conditions = no) in a 1 m x 1 m quadrat of aeolian cover, with x,y spatial resolution at 5 cm x 5 cm.

Together, the above models confirm the critical importance of the spatial correlation of sand and alabaster micro-habitats both being present as providing the set of conditions with the highest likelihood for BSC biosignatures (i.e., 'habitability'). As Supplementary Table 4d shows, when *only* sand is present, BSC biosignatures is 13 times more likely to be present versus 11,292 times higher likelihood when the sand/alabaster 'mix' (i.e., both sand and alabaster are present in same sample area) is included in the model (Supplementary Table 4c). When alabaster *only* is considered (Supplementary Table 4d), there is a 151 times lower likelihood of BSC biosignatures being present, compared to 5 times less likely odds in the alabaster plus alabaster/sand mix.

These results confirm that while the presence of a sand micro-habitat is important for BSC colonization, it is when a sand micro-habitat is co-located with or adjacent to alabaster that the likelihood of observing BSC biosignatures is greatest. The findings in Supplementary Table 4 above are perhaps more easily understood when mapped visually in a BSC probability contour map (Fig. 5d, center box). When sand is co-located with alabaster (bottom half of Fig. 5d, center box), an 11,292 times greater likelihood ('biotic hotspot') of observing BSC biosignatures exists. When only sand is present but in proximity to (but not co-located with) alabaster there is still a 13 times higher likelihood to observe BSC biosignatures than when no sand was present. Alternatively, when the sand sample was *not* co-located with or adjacent to alabaster, then sand remained overwhelmingly uncolonized by BSC (i.e., top half of Fig. 5d, center box). Thus, a positive correlation between the co-occurrence of sand (or Type I crystals) and alabaster and BSC biosignatures existed [(Fig. 5 d, center box, right-tailed t-test, $t(61)=10.697$, $p<0.001$); Fig. 5 d, center box, two-tailed t-test, $t(87)=43.254$, $p<0.001$, Supplementary Table 4 above)].

CNN Models Supplementary Data

A

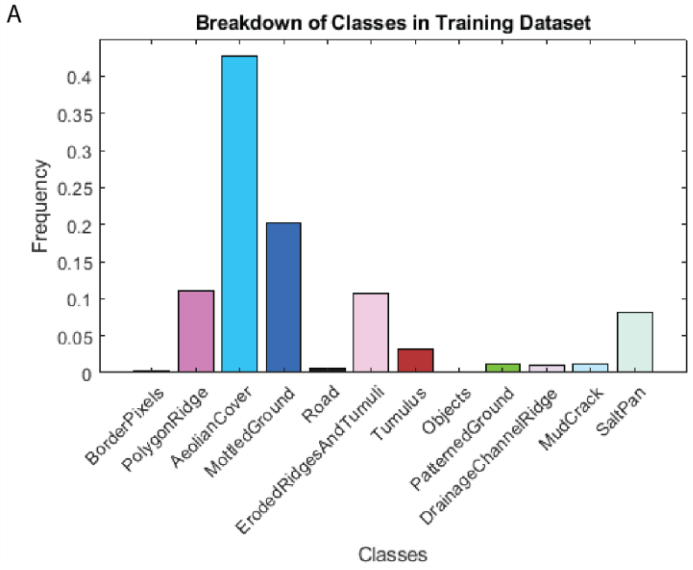

B

Class	Fraction of Total Area
Polygon Ridge	10.99%
Aeolian Cover	42.59%
Mottld Ground	20.24%
Road	0.76%
Eroded Ridges and Domes	10.59%
Domes	3.02%
Patterned Ground	1.13%
Drainage Channel Ridge	1.01%
Mud Crack	1.13%
Salt Pan	8.52%
	100.00%

Supplementary Fig. 5. Class distribution in the training set for overhead FCN analysis. A) graphical representation of the relative frequency of each class in the training set. B) Values corresponding to the plot in part A. An inversely proportional weighting scheme was applied during training to account for the unequal distribution of classes in the training set.

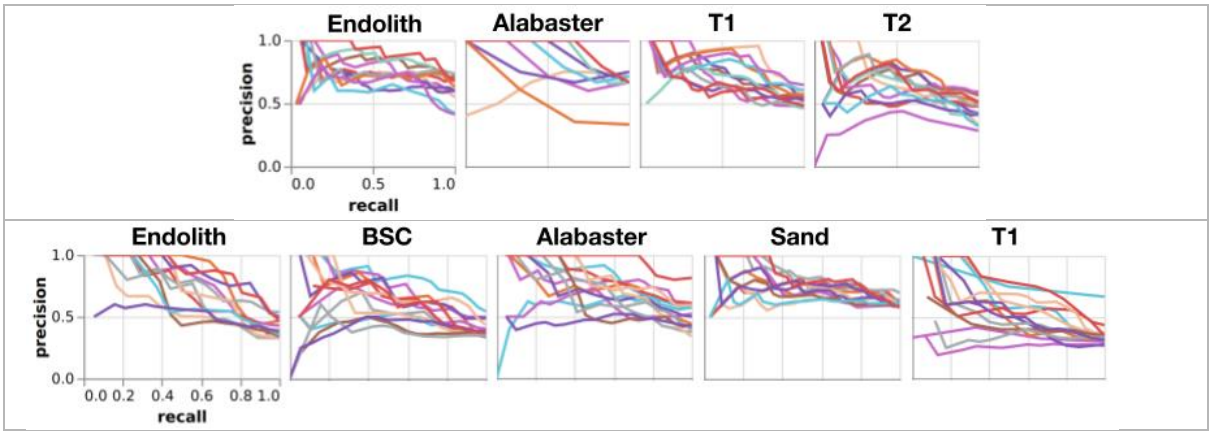

Supplementary Fig. 6. Recall-Precision curves, by macrohabitat and label, show the variability across the 10 randomized runs. Each run uses a different randomized training/validation/test split (see Supplementary Fig. 7). Top: dome macrohabitat. Bottom: aeolian cover macrohabitat. Recall = True Positives / [True Positives + False Negatives]. Precision = True Positives / [True Positives + False Positives].

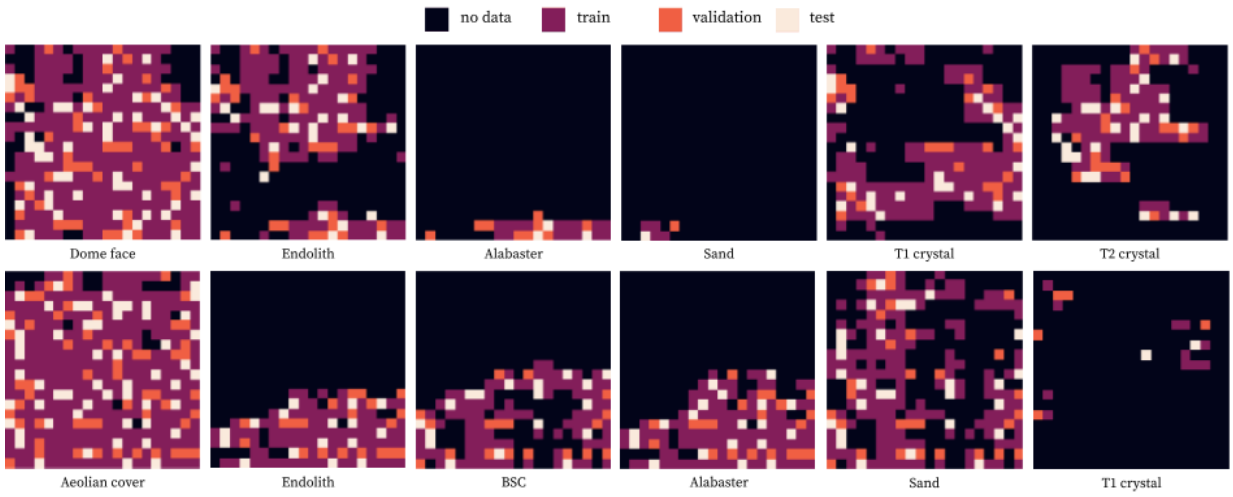

Supplementary Fig. 7. One example of 10 randomized partitions (also referred to as "splits") of macrohabitats into training, validation, and test sets. Left-most column shows the split across the entire macrohabitat. Right-most columns show the split within cells containing the label. Top: training/validation/test split in the dome macrohabitat. Bottom: training/validation/test split in aeolian cover macrohabitat. Training sets are shown in purple, validation in orange, test in white.

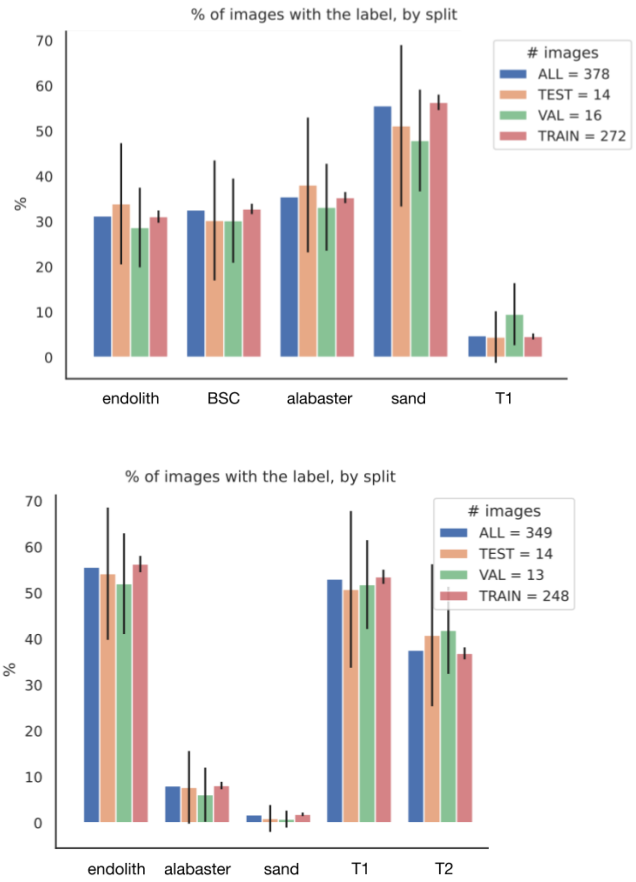

Supplementary Fig. 8. Percentage of images by label and by split. Top: Aeolian cover macrohabitat. Bottom: dome macrohabitat. Bars shown in red, green, orange are the % of training, validation, test images, respectively, by label. Bars shown in blue are the union of train, validation, and test images (i.e. the entire macrohabitat). Each randomized split (see Supplementary Fig. 7 for examples) creates a different distribution of labels in the training, validation and test sets. The bar heights measure the average percentage across 10 randomized splits, and the black vertical bars are ±1 std. deviation from the average percentage. The bar plots show that the label distributions (red, orange, green bars) are consistent with the macrohabitat distribution (blue bars). The set sizes do not change across all randomized splits. The absolute counts are shown in the legends.

Full Reference List

1. Hays, L. *et al.* Biosignature preservation and detection in Mars analog environments. *Astrobiology* **17**, 363-400 (2017).
2. Des Marais, DJ. The biogeochemistry of hypersaline microbial mats. *Advances Microbial Ecology*, **14**, 251-274 (1995).
3. Allwood, A., Walter, M., Burch, I. & B. Kamber. 3.43 billion-year-old stromatolite reef from the Pilbara Craton of Western Australia: Ecosystem-scale insights to early life on Earth. *Precambrian Research*, **158**, 198-227 (2007).
4. Al-Najjar, M., Ramette, A., Kühl, M., Hamza, W., Klatt, J. & L. Polerecky. Spatial patterns and links between microbial community composition and function in

cyanobacterial mats. *Frontiers in Microbiology*, **5**, 406, 1-11 (2014). Doi:10.3389/fmicb.2014.00406.

5. Summons, R. *et al*., Preservation of Martian organic and environmental records: Final report of the Mars biosignature working Group. *Astrobiology*, **11**, 157-181 (2011).
6. Farmer, J. & DJ Des Marais. Exploring for a record of ancient Martian life. *Journal Geophysical Research* **104** (E11), 26,977-26,995 (1999).
7. Stoker et al., We should search for extant life on Mars in this decade, BAAS, Vol 53, Issue 4, Planetary/Astrobiology Decadal Survey 2023-2032, Whitepapers #112.
8. Green, J., Hoehler, T., Neveu, M., Domagal-Goldman, S., Scalice, D. & M. Voytek. Call for a framework for reporting evidence for life beyond Earth. *Nature* **598**, 575-579 (2021).
9. Jakowsky, B. Byrne, S., Calvin, W., Curry, S., Ehlmann, B., Eignebrode, J., Hoehler, T., Horgon, B. et al. Mars, the Nearest Habitable World—A Comprehensive Program for Future Mars Exploration, BAAS, Vol. 53, Planetary/Astrobiology Decadal Survey 2023-2032, Whitepapers #112.
10. Allwood, A., Walter, M., Kamber, B., Marshall, C. & I. Burch. Stromatolite reef from the early Archaean era of Australia. *Nature*, **441**, 714-718 (2006). Doi:101038/nature04764.
11. Houghton, J., Fike, D., Druschel, G., Orpha, V., Hoehler, T. & DJ Des Marais. Spatial variability in photosynthetic and heterotrophic activity drives locale δ13Corg fluctuations and carbonate precipitation in hypersaline microbial mats. *Geobiology*, **12**, 557-574 (2014).
12. Meslier, V., Casero, M., Dailey, M., Wierzchos, J., Ascasco, C., Artieda, O., McCullough, P. & DiRuggiero, J. Fundamental drivers for endolithic microbial community assemblies in the hyperarid Atacama Desert. *Environmental Microbiology*, **20**(5), 1765-1781 (2018). Doi:10.111/1462-2920.14106.
13. Belnap, J. Welter, J., Grimm, N., Barger, N. & Ludwig, J. Linkages between microbial and hydrologic processes in arid and semiarid watersheds. *Ecology* **86**(2), 298-307 (2005).
14. Finstad, K., Probst, A., Thomas, B., Anderson, G., Demergasso, C., Echeverria, A., Amundson, R. & Banfield, J. Microbial Community Structure and the Persistence of Cyanobacterial Populations in Salt Crusts of the Hyperarid Atacama Desert from Genome-Resolved Metagenomics. *Frontiers in Microbiology* **8**, 1435. doi: 10.3389/fmicb.2017.01435 (2017).
15. Dillon, J., Miller, S., Bebout, B., Hullar, M., Pinel, N. & D. Stahl. Spatial and temporal variability in a stratified microbial mat community. *FEMS Microbiology Ecology*, **68**, 46-58 (2009).
16. Rillig, M. & J. Antonovics. Microbial biospherics: The experimental study of ecosystem function and evolution. *PNAS*, **116**, 11093-11098 (2019). Doi:10.1073/pnas.1904326116.
17. Sephton, M., & Carter, J. The chances of detecting life on Mars. *Planetary Space Science* **112**, 15-22 (2015).
18. Naveh, Z., & Lieberman, A. S. Landscape ecology: theory and application. Springer Science & Business Media. (2013).
19. Mony, C., Vandenkoornhuyse, P., Bohannan, B. J.M., Peay K. & Leibold, M. A. A landscape of opportunities for microbial ecology research. *Frontiers Microbiology* **11**, 2964, doi:10.3389/fmicb.2020.561427 (2020).

20. Hinman, N. *et al.* Surface morphologies in a Mars analog Ca-sulfate Salar, High Andes, Northern Chile. Frontiers Astronomy Space Science, doi:10.3389/fspas.2021.797591 (2022).
21. Cabrol, N., Feister, U., Häder, D. P., Piazena, H., Grin, E. & Klein, A. Record solar UV irradiance in the tropical Andes. *Frontiers Environmental Science* **2**, 1-19, doi:10.3389/fenvs.2014.00019 (2014).
22. Flahaut, J., Martinot, M., Bishop, J. L., Davies, G. R. & Potts, N. J. Remote sensing and in situ mineralogic survey of the Chilean salars: An analog to Mars evaporate deposits? *Icarus* **282**, 152-173 (2017).
23. Wierzchos, J., DiRuggiero, J., Vitek, P., Artieda, O., Souza-Egipsy, V., Skaloud, P., Tisza, M., Davila, A., Vilchez, C., Garbayo, I., & C. Ascaso. Adaptation strategies of endolithic chlorophototrophs to survive the hyperarid and extreme solar radiation environment of the Atacama Desert. *Frontiers Microbiology* **6**(934), 1-17 (2015)
24. Lynch, K., Horgon, B., Munakata-Marr, J., Hanley, J., Schneider, R., Rey, K., Spear, J., Jackson, A. & Ritter, S. Near-infrared spectroscopy of lacustrine sediments in the Great Salt Lake Desert: An analog study for Martian paleolake basins. *J. Geophysical Research Planets*, **120**, 599-623, doi:10.11002/2014.JE004707 (2015).
25. El-Maarry, M., Pommerol, A. & Thomas, N. Analysis of polygonal cracking patterns in chloride-bearing terrains of Mars: Indicators of ancient playa settings. *Journal of Geophysical Research* **113**, 2263-2278, doi:10.1002/2013JE004463 (2013).
26. Onstott, T. *et al.* Paleo-rock-hosted life on Earth and the search on Mars: A review and strategy for exploration. Astrobiology 19, 1230-1262, doi:10.1089/ast.2018.1960 (2019).
27. Davila A. & Schulze-Makuch, D. The Last Possible Outposts for Life on Mars. *Astrobiology* **16**, 159–68 (2016).
28. Osterloo, M. M. *et al.* Geologic context of proposed chloride-bearing materials on Mars. *Journal Geophysical Research* **115** (E10), 1–29 (2010).
29. Rapin, W. *et al*. An interval of high salinity in ancient Gale crater lake on Mars. *Nature Geoscience* **12**, 889-895, doi:10.1038/s41561-019-0458-8 (2017).
30. Bosak, T., Moore, K., Gong, J. & Grotzinger, J. Searching for biosignatures in sedimentary rocks from early Earth and Mars. Nature Reviews Earth and Environment 2, 490-506 (2021).
31. Balci, N., Gunes, Y., Kaiser, J., On, S, Eris, K., Garczynski, B., & Horgan, B. Biotic and abiotic imprints on Mg-rich stromatolites: Lessons from Lake Salda, SW Turkey. *Geomicrobiology Journal* **37**, 401-425, doi:10.1080/01490451.2019.1710784 (2020).
32. Williams, A., Buck, B., Soukup, D. & Merkler, D. Geomorphic controls on biological soil crust distribution: A conceptual model from the Mojave Desert (USA). *Geomorphology* **195**, 99-109, doi:10.1016/j.geomorph.2013.04.031 (2013).
33. Warren, J. *Evaporites: A Geological Compendium, Second Edition*. Springer: Berlin, 1829 pp. (2016).
34. Wierzchos, J. *et al.* Microbial colonization of Ca-sulfate crusts in the hyperarid core of the Atacama Desert: implications for the search for life on Mars. *Geobiology* **9**, 44-60, doi:10.1111/j.1472-4669.2010.00254.x (2010).
35. Robinson, C. K., Wierzchos, J., Black, C., Crits-Christoph, A., Ma, B., Ravel, J., Ascaso, C., Artieda, O., Valea, S., Roldán, M., Gómez-Silva, B., & Diruggiero, J. (2013). Microbial diversity and the presence of algae in halite endolithic communities are correlated to atmospheric moisture in the hyper-arid zone of the Atacama Desert. *Environ. Microbiol.*, *17*(2): 299–315.

36. Jørgesen, B. & Des Marais, D. Optical properties of benthic photosynthetic communities: Fiber-optic studies of cyanobacterial mats. *Limnology Oceanography* **33**,99-113 (1988).
37. Szynkiewicz, A., Moore, C., Glamoclija, M., Bustos, D. & Pratt, L. Origin of coarsely crystalline gypsum domes in a saline playa environment at the White Sands National Monument, New Mexico. *Journal Geophysical Research* **115**, F02021, doi:10.1029/2009JF001592 (2010).
38. Walker, J., Spear, J. & Pace, N. Geobiology of a microbial endolithic community in the Yellowstone geothermal environment. *Nature* **434**, 1011-1013 (2005).
39. Rasuk, M. *et al*. Microbial characterization of microbial ecosystems associated to evaporites domes of gypsum in Salar de Llamara in Atacama Desert. *Microbial Ecology* **68**, 483-494 (2014).
40. Chen, L., Papandreou, G., Kokkinos, I., Murphy, K. & Yuille, A.. Semantic Image Segmentation with Deep Convolutional Nets and Fully Connected CRFs. *CoRR*, abs/1412.7062 (2015).
41. Bishop, J. L. & Murad, E. in *Volcano-Ice Interactions on Earth and Mars.* J. L. Smellie & M. G. Chapman (eds.), p. 357-370, Geological Society, Special Publication No. 202 (2002). **45**
42. Buzgar, N., Buzatu, A., & I.V. Sanislav. The Raman study of certain sulfates. *Analele Stiintificie ale Universitatii, Al. I. Cuza IASI Geologie. Tomul LV 1* (2009).
43. Jehlicka, J., Edwards, H. & Oren, A. Raman spectroscopy of microbial pigments. *Appl. Environ. Microbiol.* **80**, 3286-3295 (2014).
44. National Academies of Sciences, Engineering & Medicine. Origins, *Worlds and Life: A Decadal Strategy for Planetary Science and Astrobiology 2023-2032*. The National Academies Press (2022). doi:10.17226/26522.
45. Farmer, J. Habitability as a Tool in Astrobiological Exploration. Ch. 1 in *From Habitability to Life on Mars*, pp. 1-12. Elsevier (2018).
46. Hays, L. *et al.* Biosignature preservation and detection in Mars analog environments. *Astrobiology* **17**, 363-400 (2017).
47. Fairen, A. *et al*. Astrobiology through the ages of Mars: the study of terrestrial analogues to understand the habitability of Mars. *Astrobiology* **10**, 821 (2010).
48. Green, J., Hoehler, T., Neveu, M., Domagal-Goldman, S., Scalice, D. & M. Voytek. Call for a framework for reporting evidence for life beyond Earth. *Nature* **598**, 575-579 (2021).
49. He, K., Xiangyu, Z., Shaoqing, R. & Jian, S. Delving Deep into Rectifiers: Surpassing Human-Level Performance on ImageNet Classification. ***IEEE***, 1026-1034 (2015).
50. Adams, J.B., and Filice, A.L., 1967, Spectral reflectance 0.4 to 2.0 microns of silicate rock powders: Journal of Geophysical Research, v. 72, doi:10.1029/JZ072i022p05705.
51. Rodríguez Albornoz, C. *Geology and controls on microbiota of the Salar de Pajonales (7.209.000 - 7.226.500 N. - 510.000 – 530.000 E)*, Antofagasta, Northern Chile. Master's Thesis, Dept. Geological Science, Universidad Católica del Norte Antofagasta, Chile (2018).
52. Ercilla, O. Origin and evolution of gypsum stromatolites in salars of the Andes highlands, northern Chile. *Andean Geology* **46**, 211-222 (2018).
53. Naranjo, J., Villa, V. & Venegas, C. Geology of the Salar de Pajonales area and Cerro Moño. Antofagasta and Atacama Regions. Geological Maps of Chile Basic Geology Series No. 153 (1: 100.000). National Geological Service, Geology and Mining Subsection. ISSN 07-17-7283 (2013).

54. Schween, J., Hoffmeister, D. & Löhnert, U. Filling the observational gap in the Atacama Desert with a new network of climate stations. *Global and Planetary Change* **184**, doi:/10.1016/j.gloplacha.2019.103034 (2020).
55. Gutiérrez, F. & Cooper, A. Surface morphology of gypsum karst. *Treatise on Geomorphology* **6**, 425-437, doi: 10.1016/B978-0-12-374739-6.00114-7 (2013).
56. Bishop, J. L, Lane, M. D., Dyar, M. D., King, S. J., Brown, A. J. & Swayze, G. Spectral properties of Ca-sulfates: Gypsum, bassanite and anhydrite. *American Miner* **99**, 2105-2115 (2014).
57. Green, A., Berman, M., Switzer, P. & Craig, M. D. A transformation for ordering multispectral data in terms of image quality with implications for noise removal: *IEEE Transactions on Geoscience and Remote Sensing* **26**, 65-74 (1988).
58. Davis, W., Pater, I. & McKay, C. P. Rain infiltration and crust formation in the extreme arid zone of the Atacama Desert, Chile. *Planetary and Space Science* **58**, 616-622 (2010).
59. McKay, C. P., Friedmann, E. I., Gómez-Silva, B., Cáceres-Villanueva, L., Andersen, D. T. & Landheim, R. Temperature and moisture conditions for life in the extreme arid region of the Atacama Desert: four years of observation including the El Niño of 1997–1998. *Astrobiology* **3**, 393–406 (2003).
60. Warren-Rhodes, K., Rhodes, K., Liu, S., Zhou, P. & McKay, C. Nanoclimate environment of cyanobacterial communities in China's hot and cold hyperarid deserts. *Journal Geophysical Research* **112**, G01016, doi: 10.1029/2006JG000260 (2007).
61. Warren-Rhodes, K. *et al.* Physical ecology of hypolithic communities in the central Namib Desert: The role of fog, rain, rock habitat and light. *Journal Geophysical Research* **118**, 1-10, doi:10.1002/jgrg.20117.2013 (2013).
62. Lange, O., Kilian, E. & Ziegler, H. Water vapor uptake and photosynthesis of lichens: Performance differences in species with green and blue-green algae as phycobionts. *Oecologia* **71**, 104-110 (1986).
63. Lange, O. L., Meyer, A. & Büdel, B. Net photosynthesis activation of a desiccated cyanobacterium without liquid water in high air humidity alone. Experiments with a *Microcoleus sociatus* isolated from a desert soil crust, *Functional Ecology* **8**, 52–57 (1994).
64. Palmer, R. & Friedmann, E. I. Water relations and photosynthesis in the cryptoendolithic microbial habitat of hot and cold deserts. *Microbial Ecology* **18**, 111–118 (1990).
65. Potts, M. & Friedmann, E. Effects of water stress on cryptoendolithic cyanobacteria from hot desert rocks. *Archives Microbiology* **130**, 267–271 (1981).
66. Tracy, C., Streten-Joyce, C., Dalton, R., Nussear, K., Gibb, K. & Christian, K. Microclimate and limits to photosynthesis in a diverse community of hypolithic cyanobacteria in northern Australia. *Environmental Microbiology* **12**, 592–607, doi:10.1111/j.1462- 2920.2009.02098.x (2010).
67. Azúa-Bustos, A. *et al.* Hypolithic cyanobacteria supported mainly by fog in the coastal range of the Atacama Desert. *Microbial Ecology* **51**, 568-581, doi:10.1007/s00248-010-9784-5 (2011).
68. Rull, F. *et al.* ExoMars Raman Laser Spectrometer for ExoMars. doi:10.1117/12.896787 (2011).
69. Kontoyannis, C. G. *et al.* The Analyst 122 (1). The Royal Society of Chemistry: 33–38 (1997).
70. Lopez-Reyes, G. *et al. European Journal of Mineralogy* **25**, 721–33 (2013).

71. Hunt, G. Spectral signatures of particulate minerals in the visible and near infrared. *Geophysics* **42**, 501-513 (1977).
72. Bishop, J. L. *In*: *Remote Compositional Analysis: Techniques for Understanding Spectroscopy, Mineralogy, and Geochemistry of Planetary Surfaces*, J. L. Bishop, J. F. Bell III, & J. E. Moersch (eds.), pp. 68-101, Cambridge University Press (2019).
73. Morris, R. V. *et al.* Evidence for pigmentary hematite on Mars based on optical, magnetic and Mössbauer studies of superparamagnetic (nanocrystalline) hematite. *Journal of Geophysical Research* **94**, 2760-2778 (1989).
74. Bishop, J. L., Pieters, C. M. & Burns, R. G. Reflectance and Mössbauer spectroscopy of ferrihydrite-montmorillonite assemblages as Mars soil analog materials. *Geochimica Cosmochimica Acta* **57**, 4583-4595 (1993).
75. Levin, S. A. The problem of pattern and scale in ecology. *Ecology* **73**, 1943-1967 (1992).
76. Underwood, A. J., Chapman, M. G., & Connell, S. D.. Observations in ecology: you can't make progress on processes without understanding the patterns. *Journal of experimental marine biology and ecology* **250**, 97-115 (2000).
77. Turner, M. G.. Landscape ecology: the effect of pattern on process. *Annual review of ecology and systematics* **20**, 171-197 (1989).
78. Turner, M. G., Gardner, R. H., O'neill, R. V., & O'Neill, R. V. *Landscape ecology in theory and practice* **401**. Springer New York. (2001).
79. Wiens, J. A., Chr, N., Van Horne, B., & Ims, R. A.. Ecological mechanisms and landscape ecology. *Oikos* **66**, 369-380 (1993).
80. Urban, D., O'Neill, R., & Shugart, H. Landscape Ecology. *BioScience* **37**, 119-127 (1987). https://doi.org/10.2307/1310366
81. Underwood, A. J. et al. Experiments in ecology: their logical design and interpretation using analysis of variance. Cambridge university press (1997).
82. Quinn, G. P., & Keough, M. J. Experimental design and data analysis for biologists. Cambridge university press. (2002).
83. Neyman, J., & Pearson, E. S. On the problem of the most efficient tests of statistical hypotheses. *Philosophical Transactions of the Royal Society of London, Series A* **231**, 289–337. *(*1933*).* https://doi.org/10.1098/rsta.1933.0009
84. Zar, J. H. Biostatistical analysis (5th ed.). Prentice-Hall/Pearson. (2010).
85. Ripley, B. D.. Spatial statistics. John Wiley Sons, New York. (1981).
86. Royle, J. A., & Nichols, J. D. Estimating abundance from repeated presence–absence data or point counts. *Ecology* **84**, 777-790. (2003).
87. Krebs, C. (1999). Ecological Methodology (2nd ed.) Addison-Wesley, 624 pp.
88. Warren-Rhodes, K., Dungan, J., Piatek, J. & McKay, C. Ecology and spatial pattern of cyanobacterial community island patches in the Atacama Desert. *Journal Geophysical Research* **112**, G04S15, doi:1029/2006JG000305 (2007).
89. Belnap, J., Phillips, S., Witwicki, D. & Miller, M. Visually assessing the level of development and soil surface stability of cyanobacterially dominated biological soil crusts. *Journal of Arid Environments* **72**, 1257-1264, doi:10.1016/j.aridenv.2008.02.019 (2008).
90. Warren-Rhodes K. et al. Hypolithic Cyanobacteria, Dry Limit of Photosynthesis, and Microbial Ecology in the Hyperarid Atacama Desert. *Microb. Ecol*. **52**, 389–98 (2006).
91. Yingst, R. et al. Is a linear or a walkabout protocol more efficient when using a rover to choose biologically relevant samples in a small region of interest. *Astrobiology* **20**(3), 327-347, doi: 10.1089/ast.2019.2090 (2020).

92. Shen, J., Wyness, A., Claire, M. & Zerkle, A. Spatial variability of microbial communities and salt distributions across a latitudinal gradient in the Atacama Desert. *Microbial Ecology* **82**, 442-458, doi:10.1007/s00248-020-10672-w. (2021).
93. Barrett, J., Virginia, R., Wall, D., Parsons, A., Powers, L. & Burkins, M. Variation in biogeochemistry and soil biodiversity across spatial scales in a polar desert ecosystem. *Ecology* **85**, 3105-3118 (2004).
94. Pointing, S. B. *et al.* Highly specialized microbial diversity in hyper-arid polar desert. *Proceedings National Academy Sciences* **106**, 19964–19969 (2009).
95. Chiodini, R., Scot, D., Chamberlin, W. Galandiuk, S., Davis, B. & Glassing, A. Microbial population differentials between mucosal and submucosal intestinal tissues in advanced Crohn's disease of the ileum. *PloS ONE* 10, e0134382, doi: 10.1371/journal.pone.0134382 (2015).
96. Rivas, L. A., García-Villadangos, M., Moreno-Paz, M., Cruz-Gil, P., Gómez-Elvira, J. & Parro, V. A 200-antibody microarray biochip for environmental monitoring: searching for universal microbial biomarkers through immunoprofiling. *Analytical Chemistry* **80**, 7970–7979 (2008).
97. Sanchez-Garcia *et al.* Microbial biomarker transition in high-altitude sinter mounds from El Tatio (Chile) through different stages of hydrothermal activity. *Frontiers Microbiology* **9**, 3350, doi: 10.3389/fmicb.2018.03350 (2019).
98. Parro, V. Antibody microarray for environmental monitoring. *In:* K. Timmis (ed.). *Handbook of Hydrocarbon and Lipid Microbiology, Ch. 22.* Springer-Verlag, Berlin Heidelberg (2010).
99. Parro, V. *et al.* A microbial oasis in the hypersaline Atacama subsurface discovered by a life detector chip: implications for the search for life on Mars. *Astrobiology* **11**, 969-96 (2011).
100. Blanco, Y., Moreno-Paz, M., Aguirre, J. & V. Parro. Multiplex Fluorescent Antibody Microarrays and Antibody Graphs for Microbial and Biomarker Detection in the Environment. *In*: T.J. McGenity, K.N. Timmis, K.N. & B. Nogales (eds.) *Hydrocarbon and Lipid Microbiology Protocols, Chapter 159.* Springer-Verlag Berlin Heidelberg (2017).
101. Moreno-Paz, M. *et al.* Biomarkers and metabolic patterns in the sediments of evoloving glacial lakes as a proxy for planetary lake exploration. *Astrobiology* **18**, 1041–1056 (2018).
102. Ekwealor, J. & Fisher, K. Life under quartz: Hypolithic mosses in the Mojave Desert. *PLoS ONE* **15**, e0235928, doi.org/10.1371/journal.pone.0235928(2020).
103. Williams, A., Buck, B. & Beyene, M. Biological soil crusts in the Mojave Desert, USA: Micromorphology and pedogenesis. *Soil Science Society America* **76**, 1685-1695, doi:10.2136/sssaj2012.0021 (2012).
104. Roldan M., Ascaso C., Weirzchos J. (2014) Fluorescent fingerprint of endolithic phototrophic cyanobacteria living within halite rocks in the Atacama Desert. *Applied and Environmental Microbiology* **80**: 2998-3006.
105. Cockell, C. *et al*. 0.25 Ga salt deposits preserve geological signatures of habitable conditions and ancient lipids. *Astrobiology* **20**, 864-877, doi.10.1089/ast.2019.2053 (2019).
106. Ripley, B. D.. Spatial statistics. John Wiley Sons, New York. (1981).
107. Gelfand, A. E., Diggle, P., Guttorp, P., & Fuentes, M. (Eds.). Handbook of spatial statistics. CRC press. (2010).
108. Dixon, D.P.M.: Ripley's K Function. Encyclopedia of Environmetrics (2006)
109. Baddeley, A., Rubak, E. & Turner, R. Spatial point patterns: Methodology and applications with R. J. Statistical Software 75, 2, doi: 10.18637/jss.v075.b02 (2016).

110. Wood, S. *Generalized Additive Models: An Introduction with R, 2nd edition*. Chapman and Hall/CRC (2017).
111. Simon, R. & Wood, N. GAMs in Practice: mgcv. *In*: Blitzstein, J., Faraway, J., Tanner, M. & Zidek, J (eds.). *Generalized Additive Models: An Introduction with R*, Second Edition, Ch. 7. Chapman and Hall/CRC (2017). Sun, H. Endolithic microbial life in extreme cold climate: Snow is required, but perhaps less is more. *Biology* **2**, 693-701, doi: 10.3390/biology2020693 (2013).
112. Generalized Additive Models with Spatio-temporal Data: https://stat.uiowa.edu/sites/stat.uiowa.edu/files/techrep/tr396.pdf
113. LeCun, Y., Boser, B., Denker, J.S., Henderson, D., Howard, R.E., Hubbard, W. & Jackel, L. Backpropagation Applied to Handwritten Zip Code Recognition. *Neural Computation* **1(**4), 541-551 (1989).
114. Roberts, M., Driggs, D., Thorpe, M., Gilbery, J., Yeung, M., Urspring, S., Aviles-Rivero, A., Etmann, C., McCague, C., Beer, L. & Weir-McCall, R. Common pitfalls and recommendations for using machine learning to detect and prognosticate for COVID-19 using chest radiographs and CT sans. *Nature Machine Intelligence **3***(3), 199-217 (2021).
115. MacArthur, R. H., & Wilson, E. O. (2016). *The theory of island biogeography*. Princeton university press.
116. Keppel G, Van Niel KP, Wardell-Johnson GW, et al. Refugia: identifying and understanding safe havens for biodiversity under climate change. *Global Ecology and Biogeography.* 2012;21:393–404.
117. Dobrowski SZ. A climatic basis for microrefugia: the influence of terrain on climate. *Global Change Biology*. 2011;17:1022–1035.
118. Sun, H. Endolithic microbial life in extreme cold climate: Snow is required, but perhaps less is more. *Biology* **2**, 693-701, doi: 10.3390/biology2020693 (2013).
119. Archer, S., de los Ríos, A., Lee, K., Niederberger, T., Cary, C., Coyne, K., Douglas, S., Lacap-Bugler, D. & Pointing, S. Endolithic microbial diversity in sandstone and granite from the McMurdo Dry Valleys, Antarctica. *Polar Biol* **40**, 997-1006, doi:10.1007/s00300-016-2024-9 (2017).
120. Noffke, N., Gerdes, G., Klenke, T. & Krumbein, W. Microbially induced sedimentary structures—a new category *within the classification of primary sedimentary structures. Journal of Sedimentary Research*, **71**, 649–656 (2001).
121. Fierer, N. & Jackson, *R. The diversity and biogeography of soil bacterial communities. Proc. Natl Acad. Sci.*, **103**, 626-631 (2006).
122. Caruso, T., Chan, Y., Lacap, D., Lau, M., McKay, C.P. & Pointing, S.. Stochastic and deterministic processes interact in the assembly of desert microbial communities on a global scale. *ISME J.* **5**, 1406-1413, doi:10.1038/ismej.2011.21 (2011).
123. Valverde et al. Prokaryotic community structure and metabolisms in shallow subsurface of Atacama Desert playas and alluvial fans after heavy rains: Repairing and preparing for next dry period. *Frontiers Microbiology*, **10**, 1641, doi:10.3889/fmicb.2019.01641 (2019).
124. Friedmann, E.I. & Weed, R. Microbial trace-fossil formation, biogenous and aiotic weathering in the Antarctic cold desert. Science**, 236**, 703-705 (1987).
125. Maier, S., Tamm, A., Wu, D., Caesar, J., Grube, M. & Weber, B. Photautotrophic organisms control microbial abundance, diversity and physiology in different types of biological soil crusts. *The ISME Journal* **12**, 1032-1046, doi:10.1038/s41396-018-0062-8 (2018).

126. Shelhamer, E., Long J. & Darrell, T. Fully Convolutional Networks for Semantic Segmentation. *arXiv*, 1605.06211 (2016).
127. Gal, Y. & Ghahramani, Z. Dropout as a Bayesian Approximation: Representing Model Uncertainty in Deep Learning. A*rXiv* abs/1506.02142 (2016).

The SETI NAI Institute Team Members
Nathalie Cabrol, Principal Investigator
Dale Anderson, Co-Investigator
Janice Bishop, Co-Investigator
Adrian Brown, Co-Investigator
Sherry Cady, Co-Investigator
Alberto Candela, Co-Investigator
Alfonso Davila, Co-Investigaor
Gözen Ertem, Co-Investigator
Jack Farmer, Co-Investigator
Virginia Gulick, Co-Investigator
Nancy Hinman, Co-Investigator
Jeffrey Moersch, Co-Investigator
Victo Parro, Co-Investigator
Michael Phillips, Co-Investigator
Cinthya Phillips, Co-Investigator
Richard Quinn, Co-Investigator
Philippe Sarrazin, Co-Investigator
Pablo Sobron, Co-Investigator
David Summers, Co-Investigator
Kimberley Warren-Rhodes, Co-Investigator
David Wettergreen, Co-Investigator
James Wray, Co-Investigator
Kris Zacny, Co-Investigator